Free-Breathing Ungated Radial Simultaneous Multi-Slice Cardiac T1 Mapping

Johnathan V. Le, PhD,[1,2] Jason K. Mendes, PhD,[1] Konstantinos Sideris, MD,[3] Erik Bieging, MD,[3] Spencer Carter, MD,[3] Josef Stehlik, MD,[3] Edward V. R. DiBella, PhD,[1,2] and Ganesh Adluru, PhD[1,2*]

Background: Modified Look-Locker imaging (MOLLI) T1 mapping sequences are acquired during breath-holding and require ECG gating with consistent R-R intervals, which is problematic for patients with atrial fibrillation (AF). Consequently, there is a need for a free-breathing and ungated framework for cardiac T1 mapping.
Purpose: To develop and evaluate a free-breathing ungated radial simultaneous multi-slice (SMS) cardiac T1 mapping (FURST) framework.
Study Type: Retrospective, nonconsecutive cohort study.
Population: Twenty-four datasets from 17 canine and 7 human subjects (4 males, 51 ± 22 years; 3 females, 56 ± 19 years). Canines were from studies involving AF induction and ablation treatment. The human population included separate subjects with suspected microvascular disease, acute coronary syndrome with persistent AF, and transthyretin amyloidosis with persistent AF. The remaining human subjects were healthy volunteers.
Field Strength/Sequence: Pre- and post-contrast T1 mapping with the free-breathing and ungated SMS inversion recovery sequence with gradient echo readout and with conventional MOLLI sequences at 1.5 T and 3.0 T.
Assessment: MOLLI and FURST were acquired in all subjects, and American Heart Association (AHA) segmentation was used for segment-wise analysis. Pre-contrast T1, post-contrast T1, and ECV were analyzed using correlation and Bland–Altman plots in 13 canines and 7 human subjects. T1 difference box plots for repeated acquisitions in four canine subjects were used to assess reproducibility. The PIQUE image quality metric was used to evaluate the perceptual quality of T1 maps.
Statistical Tests: Paired t-tests were used for all comparisons between FURST and MOLLI, with $P < 0.05$ indicating statistical significance.
Results: There were no significant differences between FURST and MOLLI pre-contrast T1 reproducibility (25 ± 18 and 19 ± 16 msec, $P = 0.19$), FURST and MOLLI ECV (29% ± 11% and 28% ± 11%, $P = 0.05$), or FURST and MOLLI PIQUE scores (52 ± 8 and 53 ± 10, $P = 0.18$). The ECV mean difference was 0.48 with 95%CI : $(6.0 \times 10^{-4}, 0.96)$.
Conclusions: FURST had similar quality pre-contrast T1, post-contrast T1, and ECV maps and similar reproducibility compared to MOLLI.
Level of Evidence: 3
Technical Efficacy: 1

J. MAGN. RESON. IMAGING 2025;61:2587–2600.

Using the spin–lattice relaxation time (T1) as a biomarker, cardiac T1 mapping can be used to quantitatively characterize the myocardium.[1] It has shown promise in differentiating various cardiomyopathies such as acute myocardial infarction,[2] amyloidosis,[3] and Anderson-Fabry disease.[4] The modified Look-Locker inversion recovery (MOLLI) sequences have

View this article online at wileyonlinelibrary.com. DOI: 10.1002/jmri.29676

Received Apr 2, 2024, Accepted for publication Nov 26, 2024.

*Address reprint requests to: Ganesh Adluru, 729 Arapeen Drive, Utah Center for Advanced Imaging Research, Salt Lake City, UT 84108, USA. E-mail: ganeshsharma.adluru@hsc.utah.edu

From the [1]Utah Center for Advanced Imaging Research (UCAIR), Department of Radiology and Imaging Sciences, University of Utah, Salt Lake City, Utah, USA; [2]Department of Biomedical Engineering, University of Utah, Salt Lake City, Utah, USA; and [3]Department of Cardiology, University of Utah, Salt Lake City, Utah, USA

Additional supporting information may be found in the online version of this article

become the widely used method for T1 mapping.[1] The MOLLI-5(3)3 and MOLLI-4(1)3(1)2 sequences[5] used for pre-contrast and post-contrast T1 mapping have reduced the breath-hold duration to 11 heartbeats in comparison to the original MOLLI-3(3)3(3)5 sequence.[6] However, this is still often difficult for sick patients to achieve, particularly during exercise or pharmacologically induced stress. The breath-hold requirement can result in poor quality T1 maps due to inter-frame motion[7] and potential loss of slice coverage due to repeat acquisitions and longer rest period requirements required between the slice acquisitions.

Shorter sequences, such as the shortened modified Look-Locker sequence (shMOLLI)[3] and the saturation recovery single-shot acquisition (SASHA) sequence,[8] have been proposed. However, these sequences have reduced reproducibility compared to the standard MOLLI sequences.[9,10] Furthermore, current T1 mapping sequences require electrocardiogram (ECG) gating with consistent R-R intervals to produce T1 maps of diagnostic quality.

Other advanced T1 mapping sequences have been proposed to address these limitations. Wang et al[11] have developed a fast breath-held and ECG-gated multi-slice T1 mapping method using a single-shot inversion-recovery radial fast low angle shot (FLASH) sequence with a regularized model-based reconstruction for direct estimation of coil sensitivities and parameter maps. Similarly, Gensler et al[12] have developed a breath-held and ECG-gated single-shot inversion recovery sequence with an offline two-parameter T1-fitting algorithm. Another breath-held and ECG-gated radial FLASH sequence was developed by Marty et al,[13] where T1 maps were estimated using a dictionary fitting method. Although these methods reduce the breath-hold burden compared to current clinical T1 mapping methods, they still rely on ECG gating. Irregularity in the ECG signal can result in unusable cardiac T1 maps for patients with atrial fibrillation. As such, there is a need for a T1 mapping framework without ECG gating or breath-holding.

MR fingerprinting and multi-tasking methods that do not rely on ECG-gating and simultaneously estimate multiple parameters have been proposed.[14,15] Cao et al[14] used a hybrid T2/inversion recovery (IR) preparation with multi-echo readouts and a variable TR scheme for simultaneous T1, T2, T2*, and fat fraction mapping. Mao et al[15] have used a T2 prep-IR simultaneous multi-slice (SMS) fast low angle shot (FLASH) sequence and a low-rank tensor imaging model to perform T1 and T2 mapping. However, simultaneous estimation of multiple parameter maps can result in longer acquisitions and reduced accuracy and precision.[14,15]

Thus, the aims of this study were to 1) develop a T1 mapping framework that can generate near-systolic, near-diastolic, and average phase T1 maps; and 2) demonstrate the feasibility of this framework by comparing its reproducibility to conventional MOLLI sequence and show its application in normal, infarct, and amyloid hearts.

Materials and Methods

Data Acquisition and Methodology

Phantom studies were performed using the T1 Mapping and ECV Standardization Program (T1MES).[16] Animal studies were approved by the Institutional Animal Care and Use Committee, and datasets were collected from 17 canine subjects. All canine subjects were from ongoing studies related to atrial fibrillation. Table S1 in the Supplemental Material lists all canine subjects and their associated study type. Human data were acquired in accordance with the policies of the local institutional review board (IRB), and written informed consent was obtained. Seven human subjects (4 males, 51 ± 22 years; 3 females, 56 ± 19 years) were used in this work. The human population included one subject with suspected microvascular disease, one subject with acute coronary syndrome and persistent atrial fibrillation, and one subject with transthyretin amyloidosis and persistent atrial fibrillation. The remaining human subjects were healthy volunteers. All but two of the studies were performed on a Prisma 3 T MRI scanner (Siemens Healthcare, Erlangen, DE) using Siemens chest and spine coil arrays (32 total channels). One human study was performed on the Siemens 1.5 T Aera scanner, and one human study was performed on the Siemens 3 T Skyra scanner. Table S2 in the Supplemental Material lists all human subjects with their health state and the scanner used for data acquisition. Human subjects were instructed to perform shallow breathing during FURST acquisitions. This work is a retrospective, nonconsecutive cohort study.

In the proposed Free-breathing Ungated Radial SMS T1 mapping (FURST) framework, an adiabatic inversion pulse with an inversion recovery time of IRT_1 is followed by the acquisition of five blocks of 150 gradient echo (GRE) rays for each block with a short recovery time of RT_s between each block. After a long recovery time of RT_L, another acquisition of five blocks of 150 rays for each block is repeated for different inversion recovery times, IRT_2 and IRT_3, to increase the sampling of the T1 recovery curve. Five blocks of 150 rays for each block are acquired every inversion, and the three acquisitions with different inversion recovery times are repeated without ECG gating for ~60–90 seconds. Figure 1 demonstrates a schematic of the proposed sequence. A retrospective study of reducing the acquisition duration was analyzed by performing the FURST reconstruction with a varying number of inversions such that T1 maps were generated from 37%, 67%, and 100% of the acquired data, corresponding to acquisition times of 34, 58, and 96 seconds, respectively.

All FURST data used a tiny golden angle[17] radial SMS protocol[18] with a CAIPIRINHA[19] phase modulation scheme for a single set and a multiband factor of 3. The FURST acquisition parameters were repetition time (TR) = 2.50 msec, echo time (TE) = 1.29 msec, flip angle (FA) = 12°, matrix size = $288 - 448 \times 288 - 448$, reconstructed voxel size = $1.4 - 2.1 \times 1.4 - 2.1 \times 7 - 8\ mm^3$, field of view (FOV) = $260 - 360 \times 260 - 360\ mm^2$, $RT_s = 0$ msec, $RT_L = 2500$ msec, $IRT_1 = 11$ msec, $IRT_2 = 100$ msec, and $IRT_3 = 190$ msec. The MOLLI-5(3)3 and the MOLLI-4(1)3(1)2 sequences were used for pre-contrast and post-contrast T1 mapping respectively. T1 estimation for the MOLLI sequences was performed using the three-parameter model. The MOLLI-5(3)(3) and MOLLI-4(1)3(1)2 sequences with 11-heartbeat breath-holds used a steady-state free precession (SSFP) readout and the acquisition

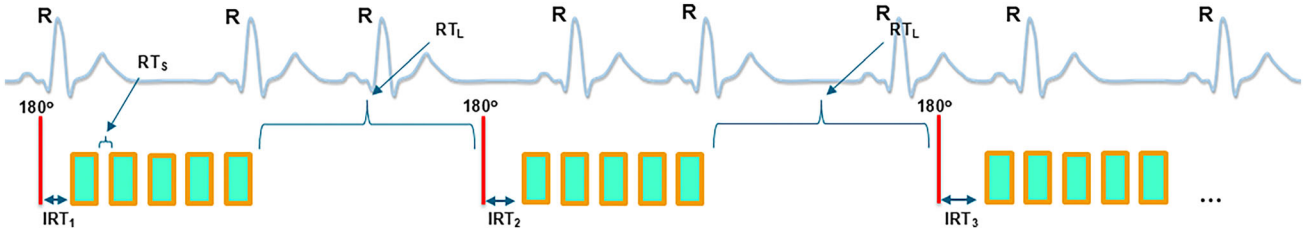

FIGURE 1: Illustration of the proposed FURST acquisition scheme. After the application of the first inversion pulse and a recovery time of IRT_1, five blocks of 150 rays for each block are acquired with a fixed short recovery time of RT_s between each block. After a fixed long recovery time of RT_L, a second inversion pulse is applied with a recovery time of IRT_2. After another fixed long recovery time of RT_L, a third inversion pulse is applied with a recovery time of IRT_3. Five blocks of 150 rays for each block are acquired every inversion, and the three acquisitions with different inversion recovery times are repeated without ECG gating for 60–90 seconds.

parameters were TR = 2.2 msec, TE = 1.12 msec, and FA = 35°, matrix size = 160 − 448 × 136 − 384, reconstructed voxel size = 0.8 − 1.8 × 0.8 − 1.8 × 7 − 8 mm^3, and FOV = 280 − 360 × 209 − 360 mm^2. FURST post-contrast T1 mapping acquisitions used the same acquisition parameters except with the following modifications: four blocks of 150 rays for each block acquired every inversion and RT_L = 1000 msec. FURST acquisition parameters were selected based on simulations and experimental acquisitions demonstrated in Fig. S1 in the Supplemental Material. Post-contrast acquisitions were performed 10–20 minutes after contrast injection using Gadoteridol (ProHance, Bracco Diagnostics, Monroe Township, USA) dose ~0.06 mmol/kg for canine subjects and Gadobutrol (Gadovist, Bayer Healthcare Pharmaceuticals, Berlin, Germany) dose ~0.075 mmol/kg for human subjects.

T1MES phantom studies were used to analyze T1 estimation between the FURST and MOLLI methods in a motion-free setting. T1MES phantom experiments with varying recovery times were also examined to assess the robustness of the dictionary pattern recognition algorithm to incomplete recovery of long T1.

T1MES phantom maps were manually segmented using a small region of interest at the center of each vial. In-vivo T1 maps were manually segmented based on the American Heart Association (AHA) 16-segment model.[20] All segmentations were performed by J.V.L. Segmented cardiac masks were used to register pre-contrast and post-contrast T1 maps using the Advanced Normalization Tools[21] to perform affine rigid registration followed by Demons deformable registration with histogram matching. ECV maps were calculated using the following Equation 1:

$$ECV = (1 - HCT)\frac{\frac{1}{T1_{myo,post}} - \frac{1}{T1_{myo,pre}}}{\frac{1}{T1_{blood,post}} - \frac{1}{T1_{blood,pre}}} \quad (1)$$

where HCT is the hematocrit measurement, $T1_{myo,post}$ and $T1_{myo,pre}$ are the post-contrast and pre-contrast T1 values of the myocardium, and $T1_{blood,post}$ and $T1_{blood,pre}$ are the post-contrast and pre-contrast T1 values of the LV blood pool. Hematocrit measurements were obtained from blood samples collected before MRI scans. Canine or human subjects that did not have hematocrit measurements were assigned a value of 45% for ECV calculations.

For coronary artery disease (CAD) assessment, pre-contrast T1 mapping can be performed during stress and rest, where the increased myocardial blood volume during stress increases T1.[22–24] This difference in stress and rest T1 values, known as the T1 reactivity, was previously tested as a potential biomarker in conjunction with late gadolinium enhancement imaging for CAD assessment.[22] In this study, we examined how the FURST method performs for stress T1 mapping in a healthy human subject. FURST and MOLLI stress T1 mapping datasets were acquired during infusing adenosine (Adenoscan, Hospira Inc., Lake Forest, USA) with a dose of 0.14 mg/kg/minute after the first 3 minutes.

Some studies have also demonstrated T1 differences between systole and diastole due to blood volume changes that could have potential diagnostic values.[25] The differences between the cardiac phase averaged T1 maps using the all-data reconstruction and systolic and diastolic T1 maps using the binned reconstruction were analyzed. MOLLI systolic T1 maps were acquired in a single subject using a manually selected delay time from the R-wave trigger based on cine imaging for quantitative comparisons with FURST systolic T1 maps.

FURST Reconstruction Pipeline

The FURST method allows for flexibility in the reconstruction pipeline, where an all-data reconstruction can generate an average cardiac phase T1 map or a binned reconstruction can generate systolic and diastolic T1 maps. In this study, the reconstruction processes for both methods are described.

PRELIMINARY RECONSTRUCTION. This reconstruction stage aims to obtain preliminary images to perform motion estimation. The images can also be used for self-gating if systolic and diastolic T1 maps are desired. For the binned reconstruction, preliminary images were obtained using a sliding window that bins the data to have 30 rays per frame. A sliding width of 15 rays was used to achieve a temporal resolution of 37.5 msec and a temporal footprint of 75 msec. For the all-data reconstruction, a higher temporal resolution is not required to capture systole or diastole for self-gating, so a sliding width of 30 rays and a temporal resolution of 75 msec was used. Gradient delay errors were estimated using the RING method[26] adapted for SMS acquisitions. The gradient delay errors were determined using the (0,0,0) phase modulated rays for a multiband factor of 3 and applied to all the rays. Preliminary images were reconstructed using a spatiotemporal constrained reconstruction (STCR) algorithm[18] described in Equation 2 below:

$$\underset{m}{\operatorname{argmin}}\frac{1}{2}\|Am-d\|_2^2+\lambda_s\left\|\sqrt{(\nabla_x m)^2+(\nabla_y m)^2+\epsilon}\right\|_1+\lambda_t\left\|\sqrt{(\nabla_t m)^2+\epsilon}\right\|_1 \quad (2)$$

The first term describes data consistency with the acquired k-space data where d is the multi-coil cartesian k-space data after gridding, and m represents the simultaneous multi-slice images to be reconstructed. Initial estimates of m were generated from interpolating radial SMS data onto a cartesian grid using simultaneous multi-slice GRAPPA operator gridding (SMS-GROG).[27] $A=\varphi DFS$ is the forward encoding matrix which describes the physics of MRI reconstruction. φ is the phase modulation matrix which modulates and demodulates SMS slices. D is the under-sampling mask describing the sampling trajectory. F is the Fourier transform and S are the coil sensitivities. The second and third terms describe the spatial and temporal total variation constraints, respectively. ε is a small positive constant to avoid singularity. The cost function in Equation 2 was minimized using an iterative method where the estimated images were updated after each iteration using the Euler–Lagrange derivative. Fifty conjugate gradient iterations were used for this optimization stage, and the regularization parameters of $\lambda_s=0.00001$, $\lambda_t=0.008$ were chosen empirically.

MOTION ESTIMATION AND SELF-GATING. In this stage, automatic motion compensation and self-gating were performed. First, frames within an inversion were averaged to estimate preliminary rigid translations between images from different inversion pulses. The estimated rigid shifts from the averaged frames were applied to all frames within their corresponding inversion. Estimates of the model-based images were generated from the preliminary rigid registered reconstructions using a dictionary pattern recognition algorithm[13] and were used for self-gating in the binned reconstruction. In the all-data reconstruction, these model-based images were used in the final motion compensation stage.

After estimating the initial model-based images, self-gating was performed for the binned reconstruction. A standard deviation map was calculated from the preliminary rigid registered images. The standard deviation map was processed with Gaussian filtering and multiplication by a 2D Gaussian function. Signal thresholding was then performed to generate cardiac masks. The model-based images were used to perform signal polarity corrections and were also subtracted from the preliminary rigid registered reconstructions to remove the signal due to inversion recovery. After multiplication with the cardiac mask and summation, the cardiac signal was generated by bandpass filtering with the cardiac motion frequency 0.5–2.2 Hz.[28,29] Figure S2 in the Supplemental Material illustrates a schematic of the self-gating procedure. The preliminary rigid registered reconstructions were then binned into systole and diastole to generate systolic and diastolic model-based images. These systolic and diastolic model-based images were used in the final motion compensation stage for the binned reconstruction.

The preliminary reconstructions (without prior registration) were then registered to their corresponding model-based images described for binned reconstruction and all-data reconstruction using a final two-step registration process, where rigid registration is performed, followed by deformable registration. During this procedure, the T1-weighted images were deformed to their corresponding one-to-one model-based images generated from the motion-free dictionary[30,31] by maximizing the normalized cross-correlation metric. The estimated rigid registration and deformable model-based registration were incorporated into a motion compensation operator for the final reconstruction stage described next. Figure S3 in the Supplemental Material illustrates a flowchart of the FURST reconstruction pipeline.

SUBSPACE-CONSTRAINED RECONSTRUCTION WITH MODEL-BASED REGULARIZATION. T1-weighted images and T1 maps were jointly reconstructed in a subspace-constrained reconstruction with model-based regularization described in Equation 3 below.[18,32]

$$\arg\min_m \frac{1}{2}\left\|AM^T(h)-d\right\|_2^2+\lambda_m\|h-B(h)\|_2^2+\lambda_s\left\|\sqrt{(\nabla_x R_x(h))^2+(\nabla_y R_y(h))^2+\varepsilon}\right\|_1$$
$$+\lambda_t\left\|\sqrt{(\nabla_t R_t(h))^2+\varepsilon}\right\|_1+\lambda_I\left\|\sqrt{(\nabla_I h)^2+\varepsilon}\right\|_1 \quad (3)$$

$$s.t.\, h=M(m) \text{ and } h=(U_k V_k)^T$$

The first term in Equation 3 describes data consistency with the acquired k-space data, where the initial estimate, m, now represents the preliminary images from the previous reconstruction stage. The second term describes model-based regularization where B is the forward operator that generates model-based images, $\hat{m}$, from the estimated T1 maps (described in the next section). M and M^T are fixed motion compensation operators that deform m to h and reform h to m for calculating the regularization and the data consistency terms, respectively. Specifically, M contains deformation fields that describe how to deform an image in m to its equivalent model-based image in $\hat{m}$ to generate the corresponding registered image in h. The subspace constraint, $h=(U_k V_k)^T$, restricts the T1-weighted images to the subspace defined by U_k. U_k are the first k temporal basis

functions and $V_k = (M(m)U_k)^T$ are the corresponding image coefficients found by projecting $h = M(m)$ onto U_k. These basis functions were generated by taking the singular value decomposition of the signal dictionary and selected based on the largest ($k = 20$) singular values. The third and fourth terms describe reordered spatial and temporal total variation constraints. R_x, R_y, and R_t are fixed operators that reorder the real and imaginary components of the images independently. The preliminary images from the first reconstruction stage were used as a prior for calculating reordering operators such that ordering the intensities makes the preliminary images from the first reconstruction stage monotonic.[33] This has been shown to preserve non-smooth varying signals,[33] which can be seen here due to repeated applications of inversion recovery pulses throughout the data acquisition. The last term describes an inversion total variation constraint that minimizes the difference between T1-weighted images acquired at the same inversion time. The cost function in Equation 3 was minimized using an iterative method where the estimated images were updated after each iteration using the Euler–Lagrange derivative. Fifty conjugate gradient iterations were used for the optimization stage and the regularization parameters of $\lambda_m = 0.05$, $\lambda_s = 0.00001$, $\lambda_t = 0.008$, and $\lambda_I = 0.004$ were empirically chosen to minimize error with the MOLLI sequences.

T1 ESTIMATION. T1 fitting was performed using a dictionary pattern recognition algorithm.[13] The dictionary for pattern recognition models the physics involving SMS reconstruction and considers the slice profile used during acquisition, similar to a previous study.[29] The dictionary also models the inversion recovery magnetization preparation and the radial GRE readout of the FURST method. The dictionary is a function of T1, TR, IRT, RT_s, RT_L, and readout flip angle with B1 0.6 : 0.1 : 1.2 to account for flip angle variations and T1 ranging from 1 : 10 : 2000 msec. Experiments modeling imperfect inversions and T2 effects in the dictionary demonstrated little difference for T1 estimation and were excluded to reduce reconstruction time and GPU memory requirements. FURST reconstructions require approximately 2–4 hours using the previously specified parameters and require approximately 24 GB of GPU memory.

Statistical Analysis

To evaluate performance, we compared T1 maps generated using the FURST method with T1 maps generated using the MOLLI-5(3)3 and MOLLI-4(1)3(1)2 sequences for pre-contrast and post-contrast datasets, respectively, using correlation and Bland–Altman plots in 13 canine and 7 human subjects. To evaluate the reproducibility of FURST and MOLLI, we examined the segment-wise T1 differences of repeated data acquisitions using pre-contrast T1 difference box plots. Repeated acquisitions were from the same imaging section using matching slice positions and acquisition parameters in four canine subjects. The FURST and MOLLI coefficient of variation for these repeated acquisitions were also compared to examine their relative variability. The perceptual quality of T1 maps was assessed using the Perception-based Image Quality Evaluator (PIQUE), a no-reference image quality metric.[34] PIQUE scores range from 0 to 100, where a lower score indicates higher perceptual quality. PIQUE scores were calculated using a manually selected region around the heart after 0–1 intensity normalization. Paired t tests were used for all statistical comparisons between FURST and MOLLI, with $P < 0.05$ indicating statistical significance.

Results

T1MES Phantom Experiments and Comparisons

Figure 2 demonstrates the performance of FURST compared to MOLLI for T1 estimation in the T1MES phantom. The FURST method shows an excellent correlation to MOLLI sequences. Figure S1 in the Supplemental Material demonstrates T1MES phantom experiments with varying recovery times between inversion pulses. The FURST method demonstrates good T1 estimation even for short recovery times despite incomplete recovery for longer T1 vials due to the dictionary pattern recognition algorithm used for T1 fitting.

In-Vivo Experiments and Bland Altman and Correlation Plots

Further comparisons are shown in Fig. 3 between FURST and MOLLI for a representative canine study. There was no significant difference between the FURST and MOLLI segment-wise pre-contrast myocardial T1 (1165 ± 25 and 1179 ± 43 msec, respectively, $P = 0.15$). The FURST method demonstrated significantly different pre-contrast blood T1 compared to MOLLI (1716 ± 30 and 1612 ± 6 msec). Figure S4 in the Supplemental Material shows a movie of the preliminary T1-weighted reconstructions, FURST T1-weighted reconstructions, and the corresponding model-based T1-weighted images for the canine subject shown in Fig. 3.

Figure 4 demonstrates segment-wise pre-contrast myocardial T1, post-contrast myocardial T1, and ECV correlations and Bland–Altman plots in 13 canine and 7 human subjects. The FURST and MOLLI segment-wise pre-contrast myocardial T1 were significantly different (1212 ± 128 and 1179 ± 87 msec). The FURST and MOLLI segment-wise post-contrast myocardial T1 were significantly different (509 ± 97 and 516 ± 92 msec). There was no significant difference between FURST and MOLLI myocardial ECV ($29\% \pm 11\%$ and $28\% \pm 11\%$, respectively, $P = 0.05$). The myocardial ECV mean difference was 0.48 with 95%CI: $(6.0 \times 10^{-4}, 0.96)$. The image quality of FURST T1 maps was similar to MOLLI T1 maps using the PIQUE image quality metric (52 ± 8 and 53 ± 10, respectively, $P = 0.18$).

T1 Difference Box Plots

Figure 5 demonstrates T1 difference box plots between FURST and MOLLI segment-wise pre-contrast myocardial T1 for repeated acquisitions in four canine subjects, where repeated acquisitions are from the same imaging section using matching slice positions and acquisition parameters. There was no significant difference between FURST and MOLLI reproducibility with T1 differences between repeat acquisitions of 25 ± 18 and 19 ± 16 msec, respectively ($P = 0.19$).

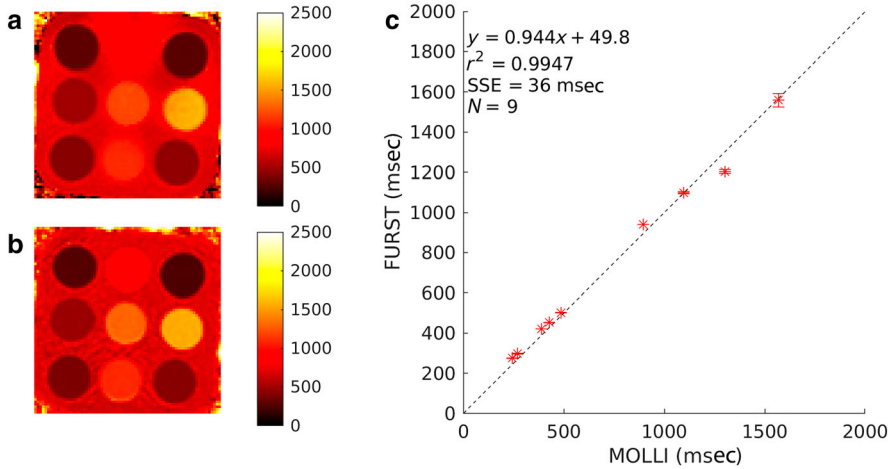

FIGURE 2: T1MES phantom results for (a) FURST, (b) MOLLI, and their corresponding (c) correlation plot. The FURST method estimates similar T1 for each of the T1MES vials ($N = 9$) compared to the MOLLI sequence.

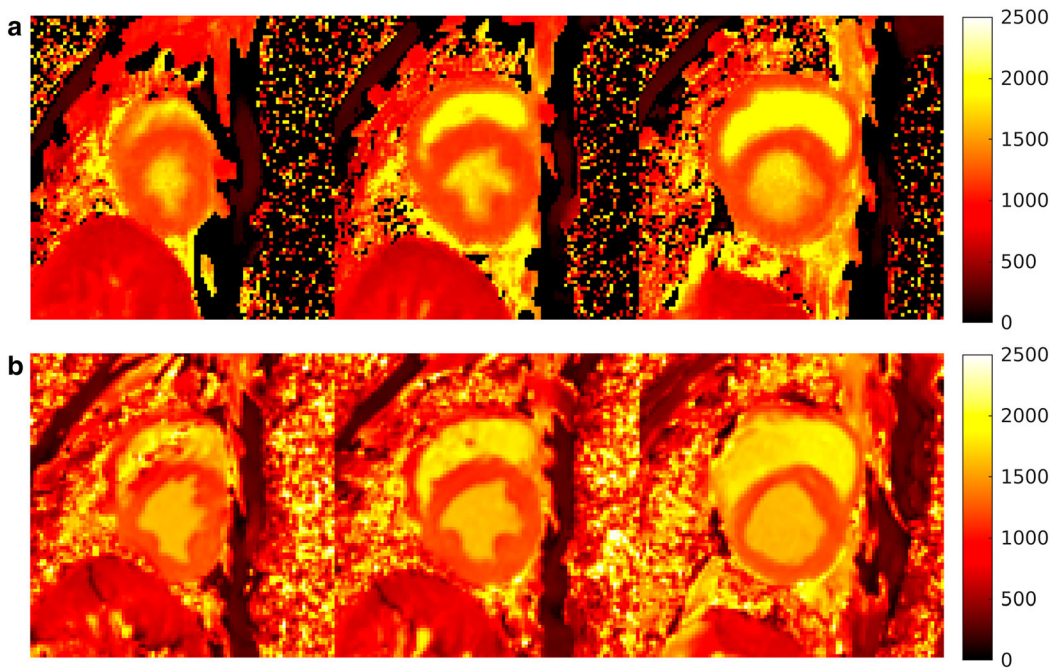

FIGURE 3: Pre-contrast T1 mapping results of (a) FURST compared to (b) MOLLI. There was no significant difference between the FURST and MOLLI pre-contrast myocardial T1 (1165 ± 25 and 1179 ± 43 msec, respectively, $P = 0.15$). FURST demonstrates significantly different pre-contrast blood T1 than the MOLLI sequence (1716 ± 30 and 1612 ± 6 msec, respectively).

The FURST and MOLLI mean coefficients of variation were 3% and 2%, respectively.

Reconstruction Flexibility

Figure 6 demonstrates cardiac phase averaged T1 maps, systolic T1 maps, and diastolic T1 maps using FURST for a normal healthy subject. The FURST averaged phase myocardial T1 was 1260 ± 31 msec. There was no significant difference between FURST and MOLLI segment-wise systolic myocardial T1 (1170 ± 35 and 1205 ± 46 msec, respectively, $P = 0.12$). There were significant differences between FURST and MOLLI segment-wise diastolic myocardial T1 (1322 ± 61 and 1219 ± 41 msec, respectively). Figure 6 also demonstrates flexibility with the FURST method, where systolic, diastolic, and cardiac phase-averaged T1 maps can be generated as needed.

Figure S5 in the Supplemental Material shows T1 maps generated using all-data reconstruction for 37%, 67%, and 100% of the acquired data. The FURST myocardial T1 generated using 37%, 67%, and 100% of the acquired data were 1283 ± 112, 1271 ± 105, and 1285 ± 98 msec, corresponding to acquisition times of 34, 58, and 96 seconds, respectively. The PIQUE scores for the FURST myocardial T1 maps were generated using 37%, 67%, and 100% of the

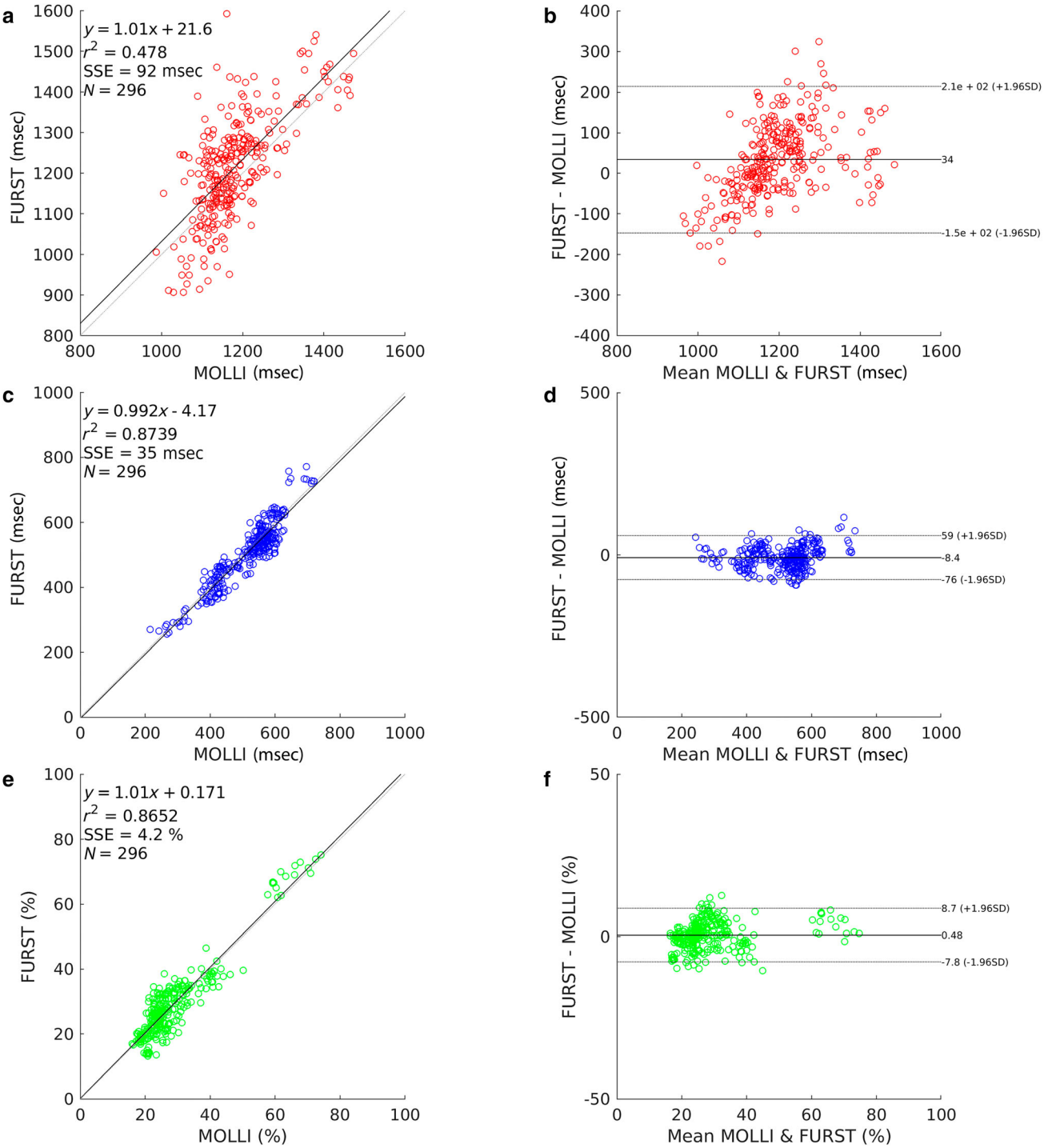

FIGURE 4: (a) Correlation and (b) Bland–Altman plots for myocardial pre-contrast T1 mapping with FURST and MOLLI in 13 canine subjects and 7 human subjects. The FURST and MOLLI pre-contrast myocardial T1 were significantly different (1212 ± 128 and 1179 ± 87 msec, respectively). (c) Correlation and (d) Bland–Altman plots for myocardial post-contrast T1 mapping with FURST and MOLLI. The FURST and MOLLI post-contrast myocardial T1 were significantly different (508 ± 97 and 516 ± 92 msec, respectively). (e) Correlation and (f) Bland–Altman plots for ECV mapping with FURST and MOLLI. There was no significant difference between FURST and MOLLI myocardial ECV ($29\% \pm 11\%$ and $28\% \pm 11\%$, respectively, $P = 0.05$). The ECV mean difference was 0.48, with 95% CI: $(6.0 \times 10^{-4}, 0.96)$. Each dot ($N = 296$) represents an averaged T1 value for an AHA segment of the myocardium.

acquired data were 59, 61, and 60, respectively. By incorporating all the data from each inversion into the T1 fitting procedure instead of systolic and diastolic binning, the acquisition time of the FURST method can be reduced to 34 seconds without discernible reductions in image quality or T1 estimation.

Stress T1 Mapping and Four-Chamber Long-Axis T1 Mapping

Figure 7 demonstrates stress pre-contrast T1 mapping and four-chamber pre-contrast T1 mapping results with FURST for the same normal healthy subject shown in Figure 6. There was no significant difference between FURST and MOLLI segment-wise stress pre-contrast myocardial T1 (1303 ± 32 and 1273 ± 46 msec, respectively, $P = 0.35$). There was no significant difference between FURST and MOLLI segment-wise myocardial T1 reactivity ($3.9\% \pm 2.8\%$ and $4.3\% \pm 2.1\%$, respectively, $P = 0.79$).

FURST demonstrates good quality T1 maps for a four-chamber long-axis slice. There was no significant difference between FURST and MOLLI segment-wise four-chamber myocardial T1 (1233 ± 35 and 1244 ± 46 msec, respectively, $P = 0.63$).

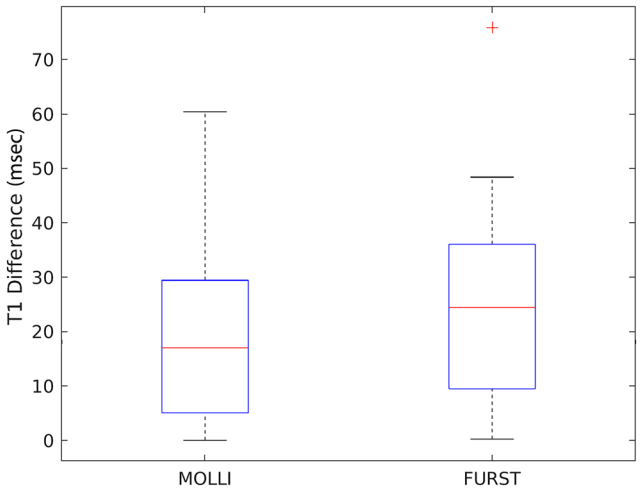

FIGURE 5: T1 difference box plots for segment-wise pre-contrast myocardial T1 between FURST and MOLLI for repeated acquisitions in four canine subjects. There was no significant difference between FURST and MOLLI reproducibility with T1 differences between repeat acquisitions of 25 ± 18 and 19 ± 16 msec, respectively ($P = 0.19$). The FURST and MOLLI mean coefficients of variation were 3% and 2%, respectively.

Human Subject with Suspected Microvascular Disease

Figure 8 demonstrates pre-contrast T1, post-contrast T1, and ECV mapping results for FURST and MOLLI in a human subject with suspected microvascular disease. In this subject, the FURST and MOLLI segment-wise pre-contrast myocardial T1 values were significantly different (1349 ± 63 and 1208 ± 59 msec, respectively), while there were no significant differences in the segment-wise post-contrast myocardial T1 values (277 ± 13 and 272 ± 29 msec, respectively, $P = 0.33$)

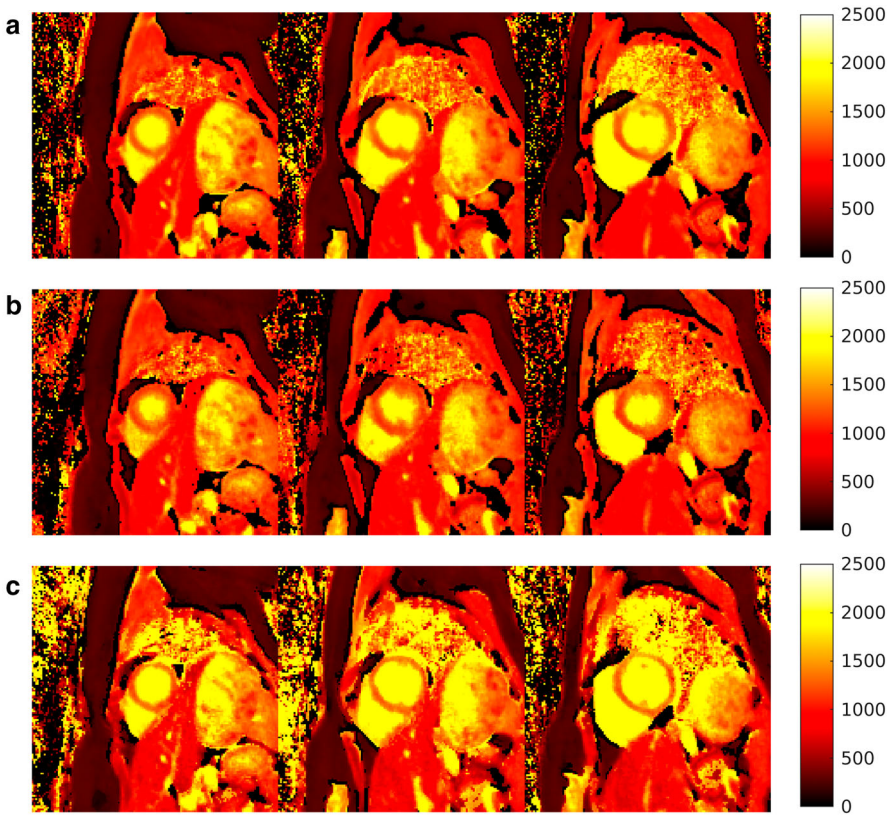

FIGURE 6: Pre-contrast T1 mapping results of FURST using (a) an all-data reconstruction to produce a cardiac phase averaged T1 map, (b) a systolic binning reconstruction to produce a systolic T1 map, and (c) a diastolic binning reconstruction to produce a diastolic T1 map. The FURST averaged phase myocardial T1 was 1260 ± 31 msec. There was no significant difference between FURST and MOLLI segment-wise systolic pre-contrast myocardial T1 (1170 ± 35 and 1205 ± 46 msec, respectively, $P = 0.12$). There were significant differences between FURST and MOLLI segment-wise diastolic pre-contrast myocardial T1 (1322 ± 61 and 1219 ± 41 msec, respectively).

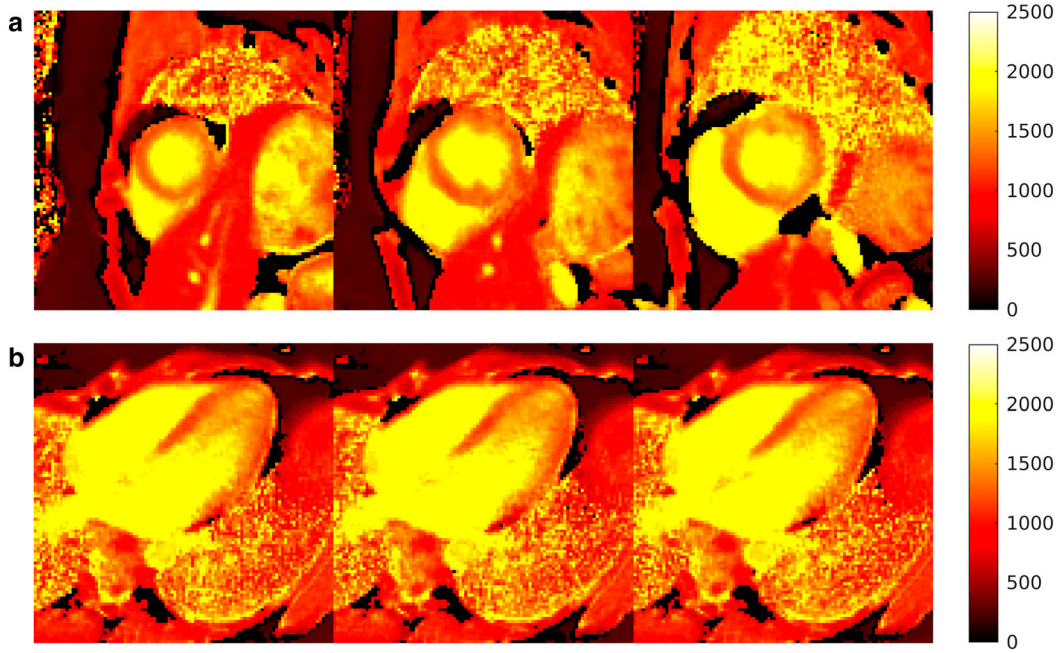

FIGURE 7: (a) Stress pre-contrast short-axis and (b) rest pre-contrast four-chamber long-axis T1 mapping results of FURST for the same normal healthy subject demonstrated in Fig. 6. There was no significant difference between FURST and MOLLI segment-wise stress pre-contrast myocardial T1 (1303 ± 32 and 1273 ± 46 msec, respectively, $P = 0.35$). There was no significant difference between FURST and MOLLI segment-wise myocardial T1 reactivities (3.9% ± 2.8% and 4.3% ± 2.1%, respectively, $P = 0.79$). There was no significant difference between FURST and MOLLI segment-wise four-chamber myocardial T1 (1233 ± 35 and 1244 ± 46 msec, respectively, $P = 0.63$).

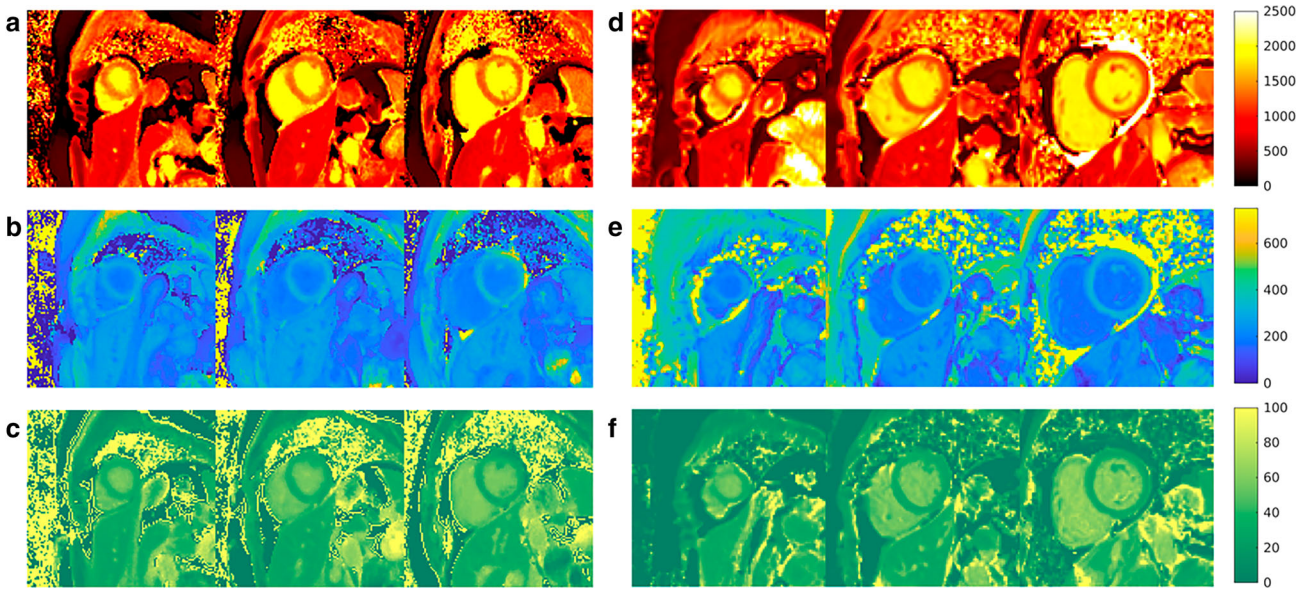

FIGURE 8: (a, d) Pre-contrast T1, (b, e) post-contrast T1, and (c, f) ECV mapping results of FURST (left) and MOLLI (right) in a human subject with suspected microvascular disease. There were significant differences between FURST and MOLLI segment-wise pre-contrast myocardial T1 (1349 ± 63 and 1208 ± 59 msec, respectively). There was no significant difference between FURST and MOLLI segment-wise post-contrast myocardial T1 (277 ± 13 and 272 ± 29 msec, respectively, $P = 0.33$). There was no significant difference between FURST and MOLLI segment-wise myocardial ECV (34% ± 2% and 32% ± 5%, respectively, $P = 0.39$).

or the segment-wise myocardial ECV (34% ± 2% and 32% ± 5%, respectively, $P = 0.39$).

Canine Subject with Myocardial Infarction

Figure 9 demonstrates pre-contrast T1, post-contrast T1, and ECV mapping results for FURST and MOLLI in a canine with an infarcted inferior wall of the left ventricular myocardium (as indicated by red arrows). Remote FURST myocardial pre-contrast T1, post-contrast T1, and ECV were 1265 ± 35 msec, 605 ± 33 msec, and 24% ± 3%. Infarct FURST myocardial pre-contrast T1, post-contrast T1, and ECV were 1228 ± 40 msec, 292 ± 6 msec, and 72% ± 2%.

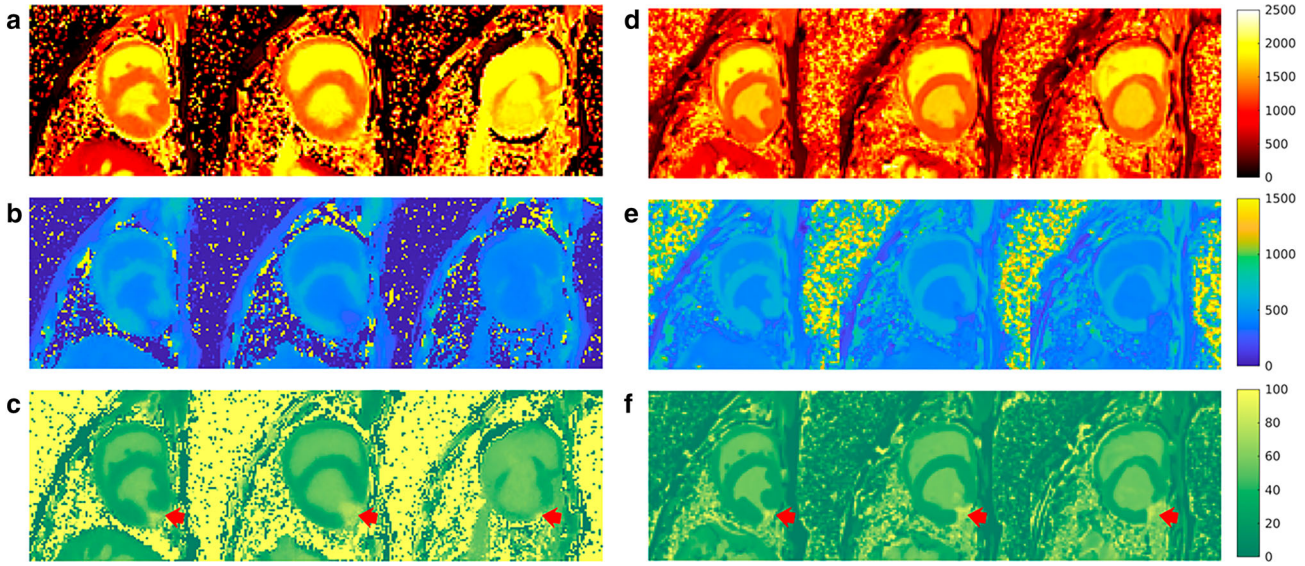

FIGURE 9: (a, d) Pre-contrast T1, (b, e) post-contrast T1, and (c, f) ECV mapping results of FURST (left) and MOLLI (right) for a canine with an infarcted inferior wall of the left ventricular myocardium (indicated by the red arrows). Remote FURST myocardial pre-contrast T1, post-contrast T1, and ECV were 1265 ± 35 msec, 605 ± 33 msec, and 24% ± 3%. Infarct FURST myocardial pre-contrast T1, post-contrast T1, and ECV were 1228 ± 40 msec, 292 ± 6 msec, and 72% ± 2%. Remote MOLLI myocardial pre-contrast T1, post-contrast T1, and ECV were 1226 ± 31 msec, 623 ± 16 msec, and 24% ± 2%. Infarct MOLLI myocardial pre-contrast T1, post-contrast T1, and ECV were 1128 ± 27 msec, 307 ± 27 msec, and 78% ± 7%, respectively.

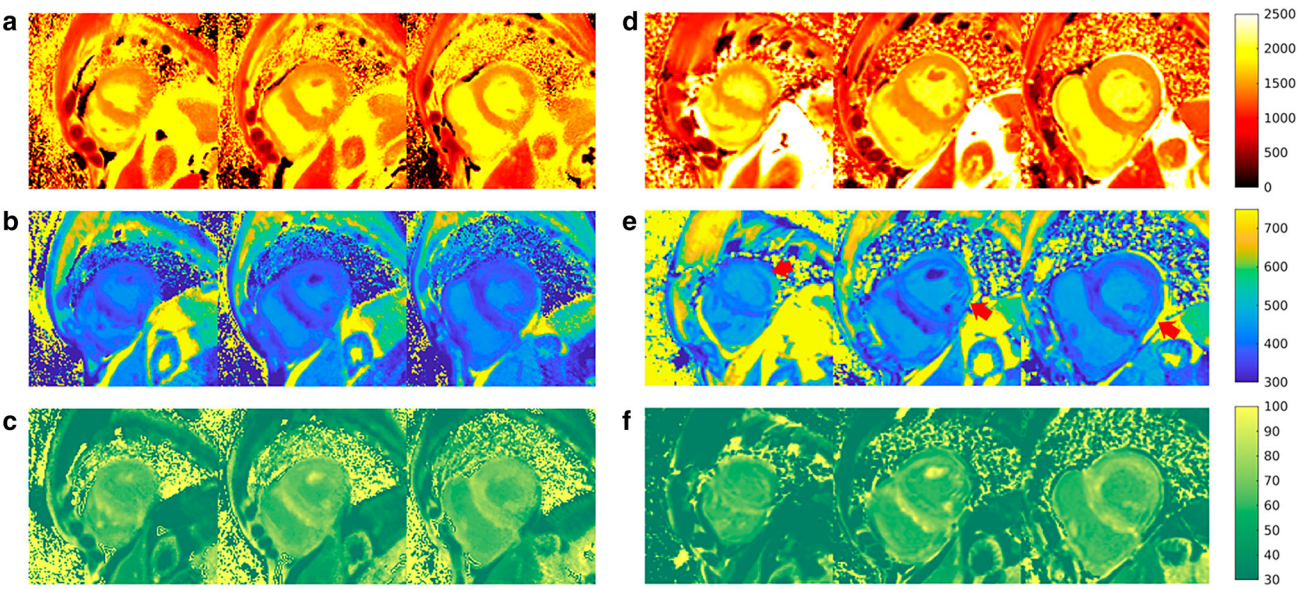

FIGURE 10: (a, d) Pre-contrast T1, (b, e) post-contrast T1, and (c, f) ECV mapping results of FURST (left) and MOLLI (right) for a patient with transthyretin amyloidosis and persistent atrial fibrillation causing varying R-R interval and poor ECG signal. There was no significant difference between FURST and MOLLI segment-wise pre-contrast myocardial T1 (1483 ± 105 and 1420 ± 41 msec, respectively, $P = 0.09$). There were significant differences between FURST and MOLLI segment-wise post-contrast myocardial T1 (381 ± 22 and 406 ± 23 msec, respectively). There were significant differences between FURST and MOLLI segment-wise myocardial ECV (68% ± 4% and 65% ± 5%, respectively). MOLLI post-contrast T1 maps demonstrate motion-related artifacts (as indicated by red arrows) due to persistent atrial fibrillation. In contrast, FURST post-contrast T1 maps demonstrate good quality regardless of varying R-R intervals and poor ECG signal.

Remote MOLLI myocardial pre-contrast T1, post-contrast T1, and ECV were 1226 ± 31 msec, 623 ± 16 msec, and 24% ± 2%. Infarct MOLLI myocardial pre-contrast T1, post-contrast T1, and ECV were 1128 ± 27 msec, 307 ± 27 msec, and 78% ± 7%.

Human Subject with Transthyretin Amyloidosis (ATTR) and Atrial Fibrillation

Figure 10 demonstrates pre-contrast T1, post-contrast T1, and ECV mapping results for FURST and MOLLI in a patient with transthyretin amyloidosis and persistent atrial

fibrillation, causing varying R-R interval and poor ECG signal. There was no significant difference between FURST and MOLLI segment-wise pre-contrast myocardial T1 (1483 ± 105 and 1420 ± 41 msec, respectively, $P = 0.09$). There was a significant difference between FURST and MOLLI segment-wise post-contrast myocardial T1 (381 ± 22 and 406 ± 23 msec, respectively) and segment-wise myocardial ECV ($68\% \pm 4\%$ and $65\% \pm 5\%$, respectively).

Discussion

In this study, the FURST method tended to produce higher T1 values for longer T1 than MOLLI. Since the MOLLI sequences are known to underestimate T1,[35,36] the FURST overestimation can be partially explained by the three-parameter model typically used for T1 estimation with the MOLLI sequences. The MOLLI SSFP readout drives recovery to reach a steady state that is less than equilibrium magnetization, resulting in an apparent recovery time of $T1^*$ which is less than the actual T1. The Look-Locker correction factor is derived from a FLASH readout that results in imperfect correction from $T1^*$ to T1.[37] Additionally, the linear cartesian phase encoding typically done with the SSFP sequences has been shown to bias T1 in favor of reducing artifacts caused by transient conditions inherent at the start of acquisitions.[38,39]

*T*1 estimation differences between the FURST dictionary-based approach and the MOLLI three-parameter model fitting may also explain the elevated left ventricular blood *T*1 of the FURST method. The dictionary pattern recognition algorithm used to estimate T1 for the FURST method models the entire sequence acquisition, including the flip angle, longitudinal magnetization, recovery time, acquisition readout, ray number of acquisition, and B1 inhomogeneity. As a result, MOLLI is likely to be more sensitive to incomplete recovery of longer T1 than FURST. This may cause MOLLI to underestimate longer pre-contrast T1 at higher heart rates.[35] Similar to FURST, a recent study has also demonstrated elevated T1 compared to MOLLI using a cartesian dictionary-based approach.[40]

We have shown that FURST T1 maps demonstrate PIQUE image quality scores similar to MOLLI T1 maps. However, FURST T1 maps tend to demonstrate mildly increased blurriness compared to MOLLI T1 maps under stable breath-holding and ECG. This is due to imperfect motion compensation, resulting in residual respiratory and cardiac motion. However, obtaining a suitable ECG signal and breath-hold conditions can be difficult for sick patients, particularly those with atrial fibrillation. Under these circumstances, unresolved cardiac motion due to poor ECG-gating results in motion-corrupted MOLLI T1 maps despite built-in scanner motion compensation. In the current study, FURST T1 maps have demonstrated good quality despite poor ECG and breath-hold conditions.

Although the FURST method affords reconstruction flexibility by allowing for an all-data reconstruction to generate cardiac phase averaged T1 maps or a binned reconstruction to generate systolic and diastolic T1 maps, some limitations with the binned reconstruction exist. Because the cardiac phase averaged reconstruction utilizes all the data acquired during an acquisition, these T1 maps tend to have higher reproducibility compared to systolic and diastolic T1 maps, which only use near-systolic or near-diastolic data as determined by the self-gating pipeline. Data binning also reduces the effectiveness of the inversion total variation constraint described in Equation 3, which can reduce image quality compared to the all-data reconstruction. Furthermore, the ungated acquisition of the FURST method also means that binning near-systolic and near-diastolic data could lead to insufficient sampling of the inversion recovery curve depending on the heart rate. However, in this study, the 60–90 second acquisition time of the FURST method was found to provide enough near-systolic and near-diastolic data to sufficiently sample the inversion recovery curve to produce good-quality T1 maps. It has also been demonstrated that the acquisition time of the FURST method could be reduced to 34 seconds using the all-data reconstruction without compromising image quality or T1 estimation. With these considerations, the all-data reconstruction may be more attractive than the binned reconstruction. The FURST method could be modified to improve the binned reconstruction. Randomizing the ordering of IRT_1, IRT_2, and IRT_3 after the inversion pulses can increase the likelihood that systole and diastole occur at varying locations on the T1 recovery curve. Varying the recovery time between inversion pulses can also improve T1 recovery curve sampling without negatively affecting T1 estimation because T1 estimation with the FURST method is robust to insufficient recovery of long T1. The motion compensation operator could deform the entire image set to near-systole or near-diastole, allowing all the data to be used in estimating near-systolic or near-diastolic T1 maps. However, this would eliminate the possibility of detecting T1 differences due to blood volume changes between the two phases because the non-systolic/non-diastolic frames deformed to systolic/diastolic would not contain the proper differences in blood volume.

Although some significant differences were demonstrated between FURST and MOLLI T1 estimation, the FURST method demonstrated similar patterns to MOLLI, where the expected general trends for pre-contrast T1, post-contrast T1, and ECV for focal diseases such as myocardial infarction and diffuse diseases such as transthyretin amyloidosis were similar. Infarcted myocardium demonstrates elevated ECV as expected due to tissue remodeling, causing edema and fibrosis. The FURST method preserves infarcted myocardium and contrasts infarcted and remote myocardium well. As with myocardial infarction, transthyretin amyloidosis

is expected to elevate pre-contrast T1 and ECV due to the deposition of misfolded transthyretin proteins in myocardial tissue. Significant differences between FURST and MOLLI post-contrast T1 and ECV maps for this subject can be explained by unresolved cardiac motion due to poor ECG-gating, resulting in motion-corrupted MOLLI T1 maps despite built-in scanner motion compensation. In addition, T1 reactivities found with the FURST method are similar to the reported literature T1 reactivities of $4.8\% \pm 3.1\%$[24] and $4.0\% \pm 4.8\%$[23] at 3 T. This suggests that the FURST method can potentially demonstrate similar diagnostic value as MOLLI despite the difference in T1 estimation. As previously stated, these differences may be explained by MOLLI underestimation bias due to imperfect assumptions in three-parameter modeling fitting, linear cartesian phase encoding, and elevated T1 estimation found with dictionary-based T1 estimation approaches.[40]

The continuous free-breathing and ungated acquisition of the FURST method also opens the possibility of developing a cine T1 mapping pipeline. During data acquisition, heart rate changes or arrhythmia cause varying cardiac phases in different cardiac cycles. As a result, generating T1 maps at each cardiac phase to produce a beating cine T1 map cannot be easily done. However, this issue can be resolved by fixing the number of cardiac phases for each cardiac cycle using a data sorting approach similar to the method used in a previous study.[29] With a fixed number of cardiac phases for each cardiac cycle, T1 maps can be generated at each cardiac phase to produce a beating T1 map. However, such a task is beyond the scope of this paper.

Limitations

Although FURST demonstrates high-quality reconstructions using model-based regularization, this constraint can have substantial memory requirements and long reconstruction times depending on the complexity of the dictionary. FURST reconstructions require approximately 2–4 hours. Deep learning for MRI reconstruction[41–43] has shown the potential to reconstruct high-quality images at a fraction of the time required for iterative reconstructions, and it could also be used to accelerate reconstruction times of the FURST method.

This study acquired a single set of three simultaneously excited slices for all datasets. However, the FURST framework can acquire multiple sets of multiband slices, allowing for whole heart coverage similar to other studies.[44–46]

Another limitation of this work is related to the free-breathing acquisition. Traditional T1 mapping techniques assume the excited tissue is within the excitation volume for each slice-selective radiofrequency pulse. Free-breathing acquisitions violate this assumption, which can lead to T1 estimation errors. However, for short-axis slices, respiration motion is mostly in-plane motion, and this work uses a recovery period of 2.5 seconds between each inversion. This recovery period allows the signal to recover near the same point before each inversion for tissues of interest. With these two considerations, in conjunction with deformable motion compensation to suppress motion, the effect due to free-breathing is greatly reduced. For these reasons, we used a similar dictionary pattern recognition algorithm for T1 estimation as discussed in Marty et al despite the free-breathing and ungated acquisition, and we have demonstrated that this dictionary pattern recognition T1 estimation approach can produce comparable results to the breath-hold, ECG-gated MOLLI T1 estimation.

This work also used a limited number of subjects, predominantly composed of canines, and included several disease states with single subject examples for each condition. Since the main purpose of this work was to test the feasibility of the FURST framework, we believe this range of subjects was sufficient. Future work will focus on a more rigorous analysis of the FURST framework for transthyretin amyloidosis with a larger sample size.

Conclusions

Using FURST, high-quality pre-contrast T1 maps, post-contrast T1 maps, and ECV maps have been demonstrated for clinical conditions varying from normal healthy subjects to disease states, including myocardial infarction and transthyretin amyloidosis. FURST T1 reproducibility was not significantly different from MOLLI T1 reproducibility. The FURST method was also demonstrated for stress T1 mapping in a single subject, where T1 reactivities were similar to those in previously published studies. The current study shows the potential clinical implications for a dedicated free-breathing and ungated simultaneous multi-slice cardiac T1 mapping sequence that may mitigate some of the limitations of standard T1 mapping protocols.

Acknowledgments

This work is supported by the National Institutes of Health grants S10OD01848201, R01HL162353, and R56HL162699.

Data Availability Statement

The code for the FURST method and example datasets is provided at https://github.com/gadluru.

References

1. Taylor AJ, Salerno M, Dharmakumar R, Jerosch-Herold M. T1 mapping: Basic techniques and clinical applications. JACC Cardiovasc Imaging 2016;9(1):67-81.

2. Dall'Armellina E, Piechnik SK, Ferreira VM, et al. Cardiovascular magnetic resonance by non contrast T1-mapping allows assessment of severity of injury in acute myocardial infarction. J Cardiovasc Magn Reson 2012;14:15.

3. Karamitsos TD, Piechnik SK, Banypersad SM, et al. Noncontrast T1 mapping for the diagnosis of cardiac amyloidosis. JACC Cardiovasc Imaging 2013;6(4):488-497.

4. Sado DM, White SK, Piechnik SK, et al. Identification and assessment of Anderson-Fabry disease by cardiovascular magnetic resonance noncontrast myocardial T1 mapping. Circ Cardiovasc Imaging 2013;6(3):392-398.
5. Kellman P, Wilson JR, Xue H, Ugander M, Arai AE. Extracellular volume fraction mapping in the myocardium, part 1: Evaluation of an automated method. J Cardiovasc Magn Reson 2012;14:63.
6. Messroghli DR, Radjenovic A, Kozerke S, Higgins DM, Sivananthan MU, Ridgway JP. Modified look-locker inversion recovery (MOLLI) for high-resolution T1 mapping of the heart. Magn Reson Med 2004;52(1):141-146.
7. Xue H, Shah S, Greiser A, et al. Motion correction for myocardial T1 mapping using image registration with synthetic image estimation. Magn Reson Med 2012;67(6):1644-1655.
8. Chow K, Flewitt JA, Green JD, Pagano JJ, Friedrich MG, Thompson RB. Saturation recovery single-shot acquisition (SASHA) for myocardial T(1) mapping. Magn Reson Med 2014;71(6):2082-2095.
9. Roujol S, Weingartner S, Foppa M, et al. Accuracy, precision, and reproducibility of four T1 mapping sequences: A head-to-head comparison of MOLLI, shMOLLI, SASHA, and SAPPHIRE. Radiology 2014;272(3):683-689.
10. Weingartner S, Messner NM, Budjan J, et al. Myocardial T1-mapping at 3T using saturation-recovery: Reference values, precision and comparison with MOLLI. J Cardiovasc Magn Reson 2016;18(1):84.
11. Wang X, Voit D, Roeloffs V, Uecker M, Frahm J. Fast interleaved multislice T1 mapping: Model-based reconstruction of single-shot inversion-recovery radial FLASH. Comput Math Methods Med 2018;2018:2560964.
12. Gensler D, Morchel P, Fidler F, et al. Myocardial T1: Quantification by using an ECG-triggered radial single-shot inversion-recovery MR imaging sequence. Radiology 2015;274(3):879-887.
13. Marty B, Coppa B, Carlier PG. Fast, precise, and accurate myocardial T1 mapping using a radial MOLLI sequence with FLASH readout. Magn Reson Med 2018;79(3):1387-1398.
14. Cao T, Wang N, Kwan AC, et al. Free-breathing, non-ECG, simultaneous myocardial T1, T2, T2*, and fat-fraction mapping with motion-resolved cardiovascular MR multitasking. Magn Reson Med 2022;88(4):1748-1763.
15. Mao X, Lee HL, Hu Z, et al. Simultaneous multi-slice cardiac MR multitasking for motion-resolved, non-ECG, free-breathing T1-T2 mapping. Front Cardiovasc Med 2022;9:833257.
16. Captur G, Gatehouse P, Keenan KE, et al. A medical device-grade T1 and ECV phantom for global T1 mapping quality assurance-the T(1) mapping and ECV standardization in cardiovascular magnetic resonance (T1MES) program. J Cardiovasc Magn Reson 2016;18(1):58.
17. Wundrak S, Paul J, Ulrici J, et al. Golden ratio sparse MRI using tiny golden angles. Magn Reson Med 2016;75(6):2372-2378.
18. Adluru G, McGann C, Speier P, Kholmovski EG, Shaaban A, Dibella EV. Acquisition and reconstruction of undersampled radial data for myocardial perfusion magnetic resonance imaging. J Magn Reson Imaging 2009;29(2):466-473.
19. Breuer FA, Blaimer M, Heidemann RM, Mueller MF, Griswold MA, Jakob PM. Controlled aliasing in parallel imaging results in higher acceleration (CAIPIRINHA) for multi-slice imaging. Magn Reson Med 2005;53(3):684-691.
20. Cerqueira MD, Weissman NJ, Dilsizian V, et al. Standardized myocardial segmentation and nomenclature for tomographic imaging of the heart: A statement for healthcare professionals from the Cardiac Imaging Committee of the Council on Clinical Cardiology of the American Heart Association. Int J Cardiovasc Imaging 2002;18(1):539-542.
21. Avants BB, Tustison NJ, Stauffer M, Song G, Wu B, Gee JC. The insight ToolKit image registration framework. Front Neuroinform 2014;8:44.
22. Liu A, Wijesurendra RS, Francis JM, et al. Adenosine stress and rest T1 mapping can differentiate between ischemic, infarcted, remote, and normal myocardium without the need for gadolinium contrast agents. JACC Cardiovasc Imaging 2016;9(1):27-36.
23. Shah R, Sree Raman K, Walls A, et al. Gadolinium-free cardiovascular magnetic resonance stress T1 mapping in patients with chronic kidney disease. JACC Cardiovasc Imaging 2019;12(10):2083-2085.
24. Yimcharoen S, Zhang S, Kaolawanich Y, Tanapibunpon P, Krittayaphong R. Clinical assessment of adenosine stress and rest cardiac magnetic resonance T1 mapping for detecting ischemic and infarcted myocardium. Sci Rep 2020;10(1):14727.
25. Tessa C, Diciotti S, Landini N, et al. Myocardial T1 and T2 mapping in diastolic and systolic phase. Int J Cardiovasc Imaging 2015;31(5):1001-1010.
26. Rosenzweig S, Holme HCM, Uecker M. Simple auto-calibrated gradient delay estimation from few spokes using radial intersections (RING). Magn Reson Med 2019;81(3):1898-1906.
27. Tian Y, Mendes J, Pedgaonkar A, et al. Feasibility of multiple-view myocardial perfusion MRI using radial simultaneous multi-slice acquisitions. PLoS One 2019;14(2):e0211738.
28. Roujol S, Tan AY, Anter E, Josephson ME, Nezafat R. Towards cardiac and respiratory motion characterization from electrophysiology data for improved real time MR-integration. J Cardiovasc Magn Reson 2013;15:P68.
29. Tian Y, Mendes J, Wilson B, et al. Whole-heart, ungated, free-breathing, cardiac-phase-resolved myocardial perfusion MRI by using Continuous Radial Interleaved simultaneous Multi-slice acquisitions at sPoiled steady-state (CRIMP). Magn Reson Med 2020;84(6):3071-3087.
30. Adluru G, DiBella EV, Schabel MC. Model-based registration for dynamic cardiac perfusion MRI. J Magn Reson Imaging 2006;24(5):1062-1070.
31. Likhite DA, Adluru G, DiBella E. *Deformable and rigid model-based image registration for quantitative cardiac perfusion*. Switzerland: Springer International; 2015.
32. Feng L, Wen Q, Huang C, Tong A, Liu F, Chandarana H. GRASP-Pro: imProving GRASP DCE-MRI through self-calibrating subspace-modeling and contrast phase automation. Magn Reson Med 2020;83(1):94-108.
33. Adluru G, Dibella EV. Reordering for improved constrained reconstruction from undersampled k-space data. Int J Biomed Imaging 2008;2008:341684.
34. Venkatanath N, Praneeth D, Chandrasekhar BM, Channappayya SS, Medasani SS. Blind image quality evaluation using perception based features. In: *21st NCC*, Piscataway, NJ. 2015.
35. McDiarmid AK, Broadbent DA, Higgins DM, et al. The effect of changes to MOLLI scheme on T1 mapping and extra cellular volume calculation in healthy volunteers with 3 tesla cardiovascular magnetic resonance imaging. Quant Imaging Med Surg 2015;5(4):503-510.
36. Zhao L, Li S, Ma X, et al. Systolic MOLLI T1 mapping with heart-rate-dependent pulse sequence sampling scheme is feasible in patients with atrial fibrillation. J Cardiovasc Magn Reson 2016;18:13.
37. Kellman P, Hansen MS. T1-mapping in the heart: Accuracy and precision. J Cardiovasc Magn Reson 2014;16(1):2.
38. Cameron D, Higgins DM, Stehning C, et al. Selection of magnetization catalyzation and readout methods for modified Look-Locker inversion recovery: A T1 mapping primer. Magn Reson Imaging 2015;33(4):363-373.
39. Cameron D, Vassiliou VS, Higgins DM, Gatehouse PD. Towards accurate and precise T(1) and extracellular volume mapping in the myocardium: A guide to current pitfalls and their solutions. MAGMA 2018;31(1):143-163.
40. Henningsson M. Cartesian dictionary-based native T(1) and T(2) mapping of the myocardium. Magn Reson Med 2022;87(5):2347-2362.
41. Aggarwal H, Mani M, Jacob M. MoDL: Model based deep learning architecture for inverse problems. IEEE Trans Med Imaging 2019;38(2):394-405.
42. Hammernik K, Klatzer T, Kobler E, et al. Learning a variational network for reconstruction of accelerated MRI data. Magn Reson Med 2018;79(6):3055-3071.

43. Le J, Tian Y, Mendes J, et al. Deep learning for radial SMS myocardial perfusion reconstruction using the 3D residual booster U-net. Magn Reson Imaging 2021;83:178-188.

44. Ma H, Zhang Y, Chen J, Yang J. Whole left ventricular coverage versus conventional 3-slice myocardial perfusion magnetic resonance imaging for the detection of suspected coronary artery disease. Acad Radiol 2019;26(4):519-525.

45. Phair A, Cruz G, Qi H, Botnar RM, Prieto C. Free-running 3D whole-heart T(1) and T(2) mapping and cine MRI using low-rank reconstruction with non-rigid cardiac motion correction. Magn Reson Med 2023;89(1): 217-232.

46. Qi H, Jaubert O, Bustin A, et al. Free-running 3D whole heart myocardial T(1) mapping with isotropic spatial resolution. Magn Reson Med 2019;82(4):1331-1342.